Uplift Capacity Evaluation of Light-framed Wood Structure's Roof-to-wall Connections

Yuanhe Li, Lihong Yao,* Yi Song, Ruijng Liu, Yueqi Wu, Siyu Chang, Xia Yu, Ziyang Zhang, and Chang Chen

The load-displacement curves of six types of roof-to-wall connection joints were obtained through uplift experiments, while the mechanical properties of each type of joint were compared and analyzed, and the applicability of each joint was verified by the Foschi load-displacement curve model simulation. The specimens were made of three kinds of wood (*Pinus sylvestris* (PS), Spruce-Pine-Fir (SPF), and Douglas fir (DF)) and two different metal connectors (A-type and B-type), and then the monotonic pullout tests were conducted on each specimen. The failure modes of each group of specimens were analyzed, and the characteristic values analysis method was used to analyze and compare the characteristic values of the load-displacement curves of each specimen, including six characteristic values: maximum load, yield load, deformation capacity, energy dissipation capacity, ductility ratio, and initial stiffness. The results showed that the load capacity of TA group (specimens with A-type metal connectors) was much greater than that of TB group (specimens with B-type metal connectors). The specimens made of DF had the best mechanical performance, but the specimens of DF group were prone to brittle failure. Finally, the fitting parameters of the Foschi model applicable to such joints were obtained.

DOI: 10.15376/biores.17.3.4532-4558

Keywords: RTWCs (Roof-to-wall connections); Metal connectors; Load-displacement curves; Characteristic values; Foschi model

*Contact information: College of Material Science and Art Design, Inner Mongolia Agricultural University, Hohhot 010018, P.R. China; *Corresponding author: yaolihong82@163.com*

INTRODUCTION

Light-frame timber constructions are extensively operated in the United States, and approximately 90% of American residential buildings are light-frame timber constructions (Yin and Li 2011). It is reported that there are plenty of light-frame timber buildings seriously damaged by severe storms, such as hurricanes and tornadoes, every year, causing incalculable economic losses (Stoner and Pang 2021). Light-frame timber building roofs are most vulnerable to damage during storm events, due to the vulnerability of low-rise roofs to large suction forces and weak roof-to-wall connections (RTWCs) (Van de Lindt *et al.* 2007; Wang *et al.* 2019a). The failure of RTWCs is the main reason for the failure of a light-frame roof, and research shows that the connectors by toe-nails are not enough to resist and transfer high wind loads in the strong wind events (Building Performance Assessment Report 1999; Cheng 2004; Morrison *et al.* 2014). Ensuring complete load paths for light-frame timber structures is key to providing adequate load transfer in wind and earthquake events, and metal connectors for RTWCs are frequently used to achieve this goal (Satheeskumar *et al.* 2017). The discontinuity of any load path in light-frame

timber structures will affect the structural performance, thereby reducing the resistance to wind and seismic forces. In addition, the discontinuity of load path may lead to damage spreading to other structural components and increase the possibility of entire failure of structural system (Shanmugam *et al.* 2009).

In reality, the storm will produce a series of peak loads with different intensities. These peaks are due to the fluctuating (turbulent) wind on the atmospheric surface, as well as the building aerodynamics, and the pressure of spatial and temporal changes on all building surfaces. The size and distribution of roof wind load depend on many parameters, such as the shape of the building, the shape of the roof, the surrounding terrain and adjacent buildings, as well as wind speed and wind direction. Building codes and typical structural analysis divide the building surface into several regions; each region has an equivalent uniform load to deal with spatial changes (Guha and Kopp 2014). It has been discovered that the metal-connectors of roof sheathing and RTWCs fail due to the accumulation of incremental damage caused by the short-duration peak of wind load (Henderson *et al.* 2013). However, the research on the pull-out resistance of various metal-connectors in RTWCs of light-frame wood structures shows that the actual carrying capacity of most metal-connectors is lower than the safety design value, which may be one of the reasons why RTWCs of wood structures cannot withstand extreme loads (Alhawamdeh and Shao 2021).

Clearly, the study on the mechanical properties of RTWCs in light-frame wood structures is a necessary part of the research on the overall structural performance. According to ASTM D1761 (2006), researchers tested the ultimate bearing capacity of RTWCs with three metal-connectors without toe-nails. It was found that the main failure modes of the three metal-connectors were steel plate tearing, wood cracking, and nail pulling or bending (Shanmugam *et al.* 2011). On the basis of this study, Edmonson *et al.* (2012) conducted a comparative study on the mechanical properties of RTWCs with various connections. They reported that the tensile mechanical properties of metal-connectors were 3.2 times than that of toe-nails. The ultimate bearing capacity of the joint combined with metal-connectors and oblique toe-nails was equal to the sum of the ultimate bearing capacity of the oblique toe-nail joints and metal-connector joints (Edmonson *et al.* 2012). Alhawamdeh evaluated the anti-uplift wind load performance of six RTWC-configurations through the monotonic uplift tests and obtained the force-displacement curves of each specimen. According to the average curves of the six joints, six characteristic parameters, including load capacity, deformation capacity, energy dissipation, ductility ratio, initial stiffness, and the coefficients of variation (COV) of the load capacities, were calculated (Alhawamdeh and Shao 2020). To determine the location of regional failure in the inclined roof of the typical light-frame wood structure, Stevenson *et al.* (2019) provided a modeling method using the finite element modeling technology to analyze the internal load effect and strength behavior of the wood structure roof components under the action of wind uplift. This method adopted the force of an envelope of the extreme member and joint forces under uplift, and compared them with unfactored strength values to produce conservative demand-to-capacity (D/C) ratios. According to the relative D/C ratios, the performance of structural components was compared and the 'weak links' were determined.

The quasi-static mechanical properties (strength and stiffness) of wood depend intensively on the type, moisture content, loading direction, wood density, and even the location inside the tree. In this study, a total of six RTWC joints were made by three kinds of wood and two typical metal connectors. The failure mode and connection performance

of the joints under extreme loads, such as strong wind, was emulated by uplift experiments, which is of great significance to the wind resistance design of light frame wood structures.

EXPERIMENTAL

Materials

In this study, three kinds of wood with rich resource reserves and wide application in light-frame wood structures were selected, namely, Douglas fir (*Pseudotsuga menziesii*), *Pinus sylvestris* L., and Spruce-Pine-Fir (SPF). Douglas fir is one of Canada's largest commercial softwood varieties with straight grain and uniform texture. Douglas fir has high hardness, strong abrasion resistance, high strength to weight ratio, and good screw holding capability, and is considered one of the strongest softwood varieties (Zhou *et al.* 2020). Therefore, it is widely used in housing frames, flooring, lining, and so on. In recent years, the global demand for Douglas fir has increased annually, and it has become one of the important sources of global large-diameter structural timber. *Pinus sylvestris* L. is widely distributed in Russia, Turkey, Mongolia, and the Greater Khingan Mountains Forest region of China. It has strong cold-resistance capability and does not require rich soil moisture conditions; thereby, it is capable for utilization as an afforestation tree species in mountainous and sand dune areas (Ekman *et al.* 2002; Korkut *et al.* 2008; Arriaga *et al.* 2012; Cai *et al.* 2016; Buyuksari *et al.* 2017; Burawska-Kupniewska *et al.* 2019; Sarkhad *et al.* 2020; Sobierajska *et al.* 2020). *Pinus sylvestris* L. has various apparent material performance, such as straight texture, clear pattern, moderate uniform structure, lightweight performance, low density, distinct rosin smell, high water resistance, high moisture resistance, good antifungal corrosion, and high durability, so it is mainly used in structural materials, and is also widely used in other wood production fields (Megnis *et al.* 2002; Yildiz *et al.* 2004; Rautiainen and Alen 2007; Temiz *et al.* 2008; Simsek *et al.* 2010; Bekhta *et al.* 2014; Witomski *et al.* 2014; Shen *et al.* 2020). The SPF is a generic term for a class of coniferous specimen lumber, mainly from the United States of America and Canada, including spruce, pine, and fir (Zhang and Cai 2008; Gong *et al.* 2014; Zheng *et al.* 2015; Wang *et al.* 2017; Zhang *et al.* 2021). It is a type of commercial softwood tree species combination wood, with white and clean material appearance, close and meticulous texture, small scar appearance, high strength to weight ratio, and strong nail holding capability (Di and Zuo 2021; Xiao *et al.* 2021). Moreover, SPF is widely used in the construction industry, and could be used in important structural components such as beams and columns (Xiao *et al.* 2017; Wang *et al.* 2019b; Dong *et al.* 2021).

The specimens were made of *Pinus sylvestris* L. (Tahe County, China), SPF (Vancouver, Canada), and Douglas fir (Vancouver, Canada). They were prepared after two weeks of natural drying until a constant mass and moisture content of 7% to 8% was reached, and the average densities of the three woods were 0.42, 0.34, and 0.44 g/cm^3, respectively. The connecting part of the toe-nails of the specimens was to take galvanized ring shank nails, compared with ordinary steel nails usually used for the connections of the top plate, to prevent the sliding phenomenon of the specimen during the connection or loading process and resulting in experimental errors.

Two types of metal connectors were selected, both of which were galvanized steel plates with a yield strength of 235 MPa and a zinc content of 275 g/m^2. Self-tapping screws were used to fix the metal connectors at the joints of the specimens. The specifications and properties of the basic materials of the specimens are shown in Table 1.

Table 1. Construction Materials Properties in Test Connections

Material		Dimensions	Description/Properties
Dimension Lumber	Wood truss and top plates	40 × 90 × 400 mm	*Pinus sylvestris* L.
			SPF
			Douglas fir
Nail	Ring shank nails	*d* = 3.5 mm; *l* = 80 mm	Level of steel (Minimum yield strength = 235 MPa)
Fastener	Hurricane ties A	2 × 40 × 164 mm	Galvanized steel sheet (Minimum yield strength = 235 MPa, Zinc content = 275 g/m^2)
	Hurricane ties B	2 × 64 × 52 × 172 mm	
	Tapping screw used to fix ties	*d* = 3.5 mm; *l* = 30 mm	Level of steel (Minimum yield strength = 235 MPa)

Specimen Design and Test Process

The specimens were made of three kinds of wood (Douglas fir, *Pinus sylvestris* L., and SPF) connected by two different metal connectors, which were generally divided into two categories: metal connector A group and metal connector B group. As a result, there were six groups of specimens in total named TA-PS, TA-SPF, TA-DF, TB-PS, TB-SPF, TB-DF, and eight specimens of each group were tested. The schematic diagram for the installation of metal connectors and joints is shown in Fig. 1. The configuration and quantity of specimens are shown in Table 2.

Table 2. Six Configurations of Specimens and Their Indices

Index	Group	Description	No. of Specimens
TA-PS	With metal connector A	*Pinus sylvestris* L.+ Nails + A (metal connector A)	8
TA-SPF		SPF + Nails + A	8
TA-DF		Douglas fir + Nails + A	8
TB-PS	With metal connector B	*Pinus sylvestris* L. + Nails + B	8
TB-SPF		SPF + Nails + B	8
TB-DF		Douglas fir + Nails + B	8

The experiment adopted a microcomputer-controlled electronic universal mechanical testing machine (Model: WDW-T100; Jinan Lilian Testing Technology Co., Ltd., Tsinan, China) with a maximum test force of 100 kN, and the specimens were fixed on the equipment by a self-made fixture in the test. The fixing method of the specimen and the mechanical testing machine in the test was to use the steel plate at the bottom of the equipment to fix the transverse wood at the bottom of the specimen on the mechanical testing machine, and the upper fixture was connected with the transverse wood at the top of the specimen, so that the specimen could move upward in the vertical direction through the loading force to simulate the uplift effect of strong wind load on the node (Fig. 2). According to ASTM D1761 (2006), monotone upward loading was completed by the displacement-control method, and the loading rate was 2.54 mm/min. The loading rate used in this paper is a general test simulation method, which is suitable for most cases. However, if the simulation is more extreme, special loading rate is needed. The relevant results under specific conditions can be estimated by converting the test results in this paper into the proportional factor of loading rate.

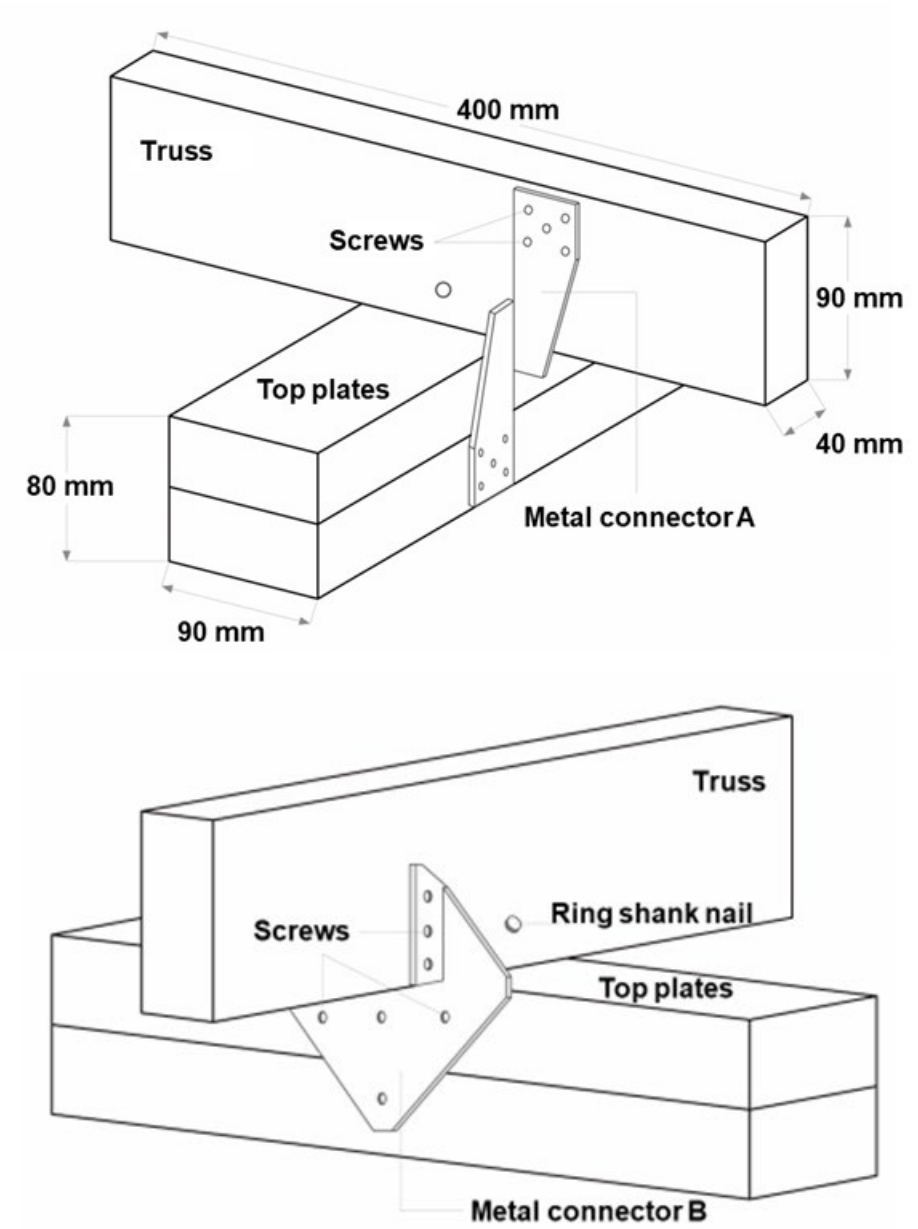

Fig. 1. The schematic diagram for the installation of specimens TA-group and TB-group

Fig. 2. The fixing method of specimen on equipment (TA-Group and TB-Group)

RESULTS AND DISCUSSION

Test Phenomena and Failure Modes

The failure modes of each group of specimens in this test are shown in Fig. 3. From Fig. 3 (a), (c), and (e), it can be realized that the specimens of three different woods connected by metal connector A were all pulled off at the side of the upper metal tensile part connecting the screw and the wood. Due to the bending deformation of the upper end of the metal connector and the stress concentration at the screw position of the cross anti-sink head, the brittle fracture failure of the specimens was caused directly. In comparison, there was basically no damage and no obvious pull-out phenomenon at the screw position on the lower end of the metal connector. As a result, the main complete failure modes of the three groups of specimens fixed with metal connector A can be summarized as follows: the screws on the upper side of the metal connector part closer to the loading end were pulled out, and the screws were bent or the wood was directly brittle fracture at the cross back-buckle position of the screw, while the lower side of the metal connector further to the loading end was basically unchanged and the screw pull-out phenomenon was not obvious.

In the TA-DF group, five out of the eight specimens had brittle fracture of screws, while the other two groups had much less brittle fractured screws after loading, because the screw holding capability of Douglas fir was much greater than that of the other two types of wood. Moreover, the wood at the truss screws of the TA-DF specimens was severely crushed and torn. In the TA-SPF group, the screws were almost completely pulled out after loading, indicating that the screw holding capability of SPF as RTWC-node was insufficient. In TA-PS group, the wood contacted with the specimen screws was seriously damaged by shear stress and most of the screws were plastically deformed, but almost no screws were completely pulled out, indicating that the screw holding capability of *Pinus sylvestris* L. was between that of Douglas fir and SPF.

From Fig. 3 (b), (d), and (f), the top plates of the specimens with metal connector B were severely split due to the large load on the rods of screws used to fix the connector during the loading process, which caused the nail rods to squeeze the wood at the top plates around them. At the same time, the shorter screws caused the wood at the nail joint to split along the wood grain and gradually expand as the displacement increased. Plastic deformation of the screws also occurred. The failure modes of specimens with metal connector B were basically the same as specimens with metal connector A during the loading process.

According to the test results of all specimens, the TA group specimen was closer to the 80% of equipment's maximum load when it was completely destroyed, while the TB group specimen was completely destroyed when it was subjected to smaller force. Therefore, it could be inferred that the geometric shape of the metal connector determined the mechanical behavior of the RTWC joint to a certain extent. Both metal connectors produced only slight deformation or almost no deformation, indicating that the metal connectors did not play a full role. In comparison, the mechanical properties of such RTWC joints strengthened with metal connectors were largely determined by the wood texture, density, moisture content, screw-holding capability, and the performance of the selected screws.

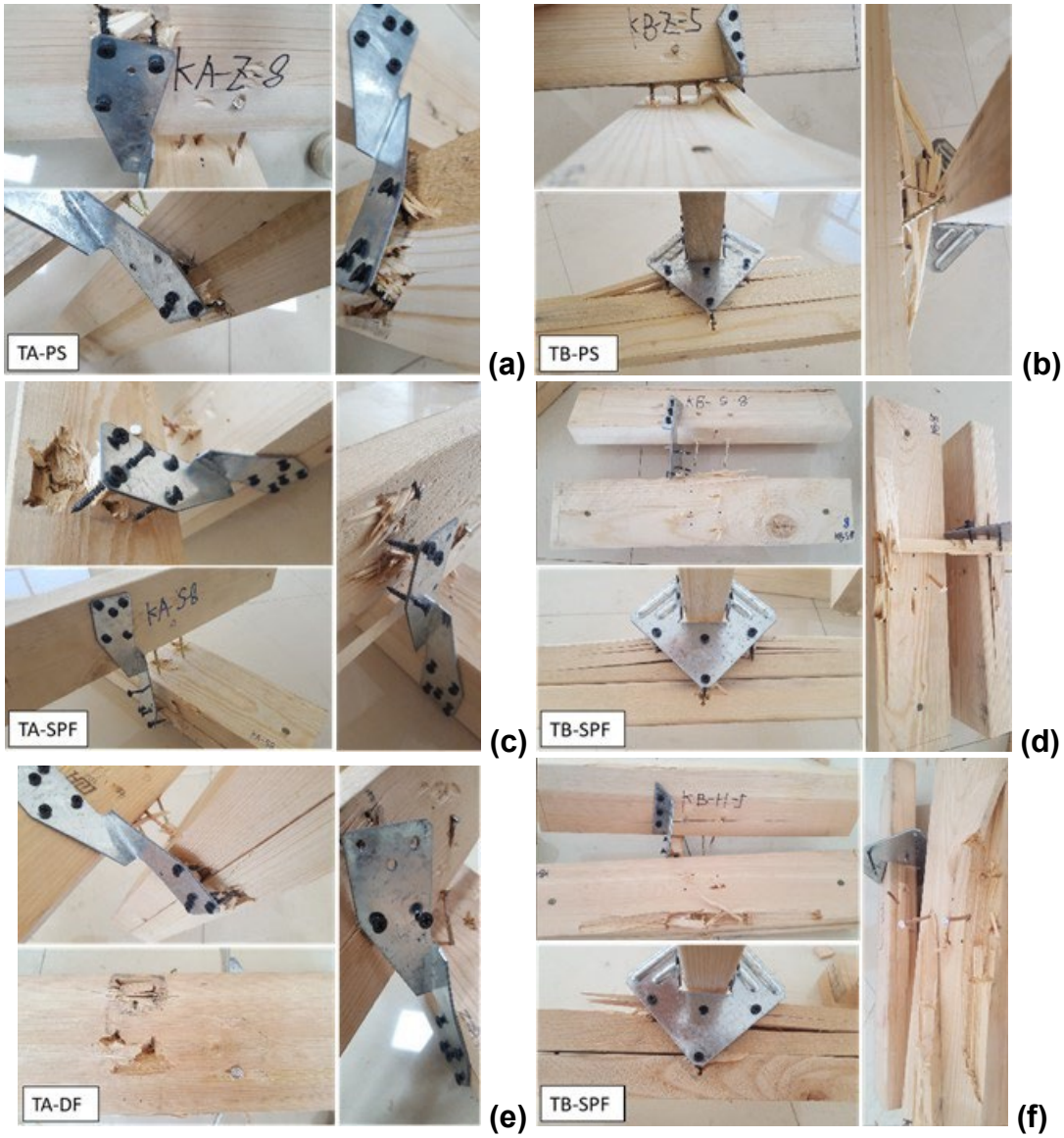

Fig. 3. Failure modes of 6 types of configurations: (a) TA-PS: *Pinus sylvestris* L.+ Nails + A (metal- connector A); (b) TB-PS: *Pinus sylvestris* L.+ Nails + B; (c) TA-SPF: SPF + Nails + A; (d) TB-SPF: SPF + Nails + B; (e) TA-DF: Douglas fir + Nails + A; (f) TB-DF: Douglas fir + Nails + B

Load Displacement Curve

The load-displacement curves of each specimen in this test are shown in Fig. 4. According to Fig. 4 (a), (c), and (e), the overall trend of load-displacement curves of the three groups of wood specimens enhanced with metal connector A were basically similar. In the initial loading phase, the load and displacement of the specimens were basically proportional to each other. When the ultimate load was reached, the specimens began to yield, and the displacement showed a rapid downward trend in the yield stage until the specimen was completely destroyed. The load-displacement curves of each specimen were fitted, and the average curves (red lines) representing the overall characteristics were obtained. The load-displacement curves of each specimen represent noticeable nonlinear characteristics throughout the loading stage. The load-displacement curves of the three groups of specimens indicate clear fluctuation during the loading process, especially after

the specimen enters the yield stage. The fluctuation was extremely obvious, which shows that the stiffness of the joint did not change apparently in the early stage, but it changed noticeably after entering the yield stage. After entering the yield stage, the stress concentration of the wood around the screw gradually splits, and gradually leads to the instability of the joint and finally the failure.

Compared with the other two groups, the load-displacement curves of the five specimens in TA-DF group begin to fluctuate in the range of 5 to 8 mm at the beginning of loading, and the curves of the other two groups are relatively smooth parabolas at the initial stage of loading. In the process of the specimen entering the yield stage until failure, the load-displacement curve of the TA-DF group was also more volatile than that of the other two groups of specimens. Because the load-displacement curve fluctuated more obviously in the entire cycle loading process, the average curve of TA-DF group is relatively less representative than that of the other two groups of specimens in the curve fitting process. Combined with the failure modes of the specimen, it can be inferred that the reason for this fluctuation in the load-displacement curve of the TA-DF group specimen is that Douglas fir has a stronger screw holding capability, so greater friction will be generated between the wood and the screw under force, which will lead to brittle fracture of the screw used to fix the metal part. Or at the beginning of the loading, the wood will split along the grain direction and the crack will gradually increase due to the stress concentration of the contact part with the screw, which will lead to the change of stiffness of the TA-DF group specimens at the initial loading stage.

According to Fig. 4 (b), (d), and (f), the overall trend of load-displacement curves of specimens reinforced with metal-connector B were similar, which begins at the initial stage and yield until failure after reaching the ultimate load. Compared with the TA group, the load of the TB group decreased relatively slowly with the increase of displacement after entering the yield stage. Combined with the failure mode, this phenomenon is due to the fact that the wood area in the TB group specimen contacted with the screw was not completely split along the grain so that the stiffness change appeared not obvious. The area of load-displacement curve envelope is proportional to the energy dissipation capacity of the specimen during loading, so it can be seen that the energy dissipation capacity of specimens in the TA group was noticeably better than that in the TB group.

Through comparing the load-displacement average curves of six configurations (Fig. 5), the ultimate bearing capacity and energy dissipation capacity of specimens with metal connector A were apparently better than those of specimens with metal connector B, and the ultimate bearing capacity of specimens with the same metal connector showed the following rule: DF group > SPF group > PS group.

The load-displacement curves of the six types all first show linear characteristics, and then show high irregularity. Therefore, it is deduced that under the condition that the force obviously exceeds the linear stress-strain range, extensive damage of RTWC joints may occur when the building is subjected to very strong wind.

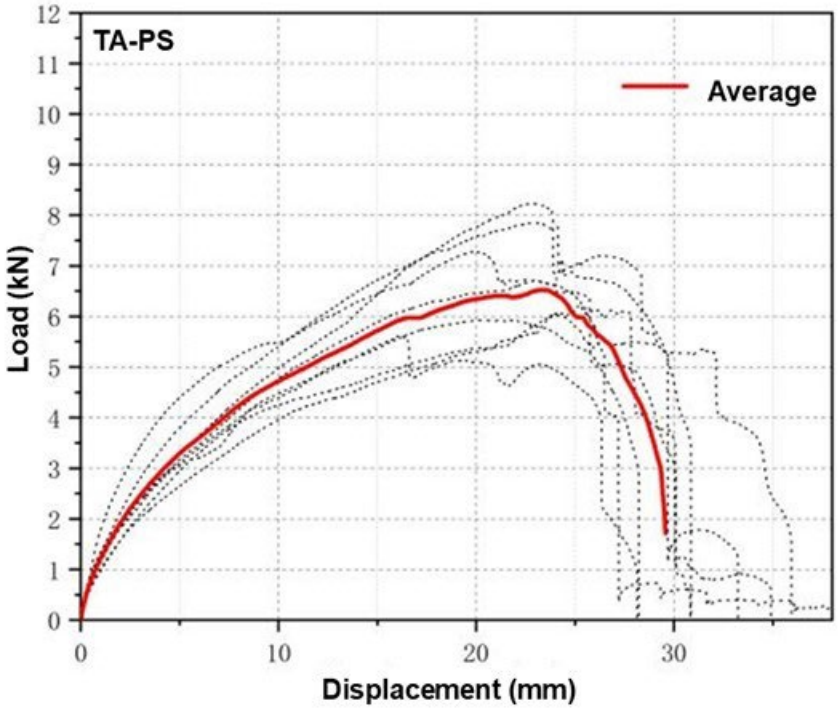
TA-PS
Average
Load (kN)
Displacement (mm)
0
1
2
3
4
5
6
7
8
9
10
11
12
0
10
20
30

(a)

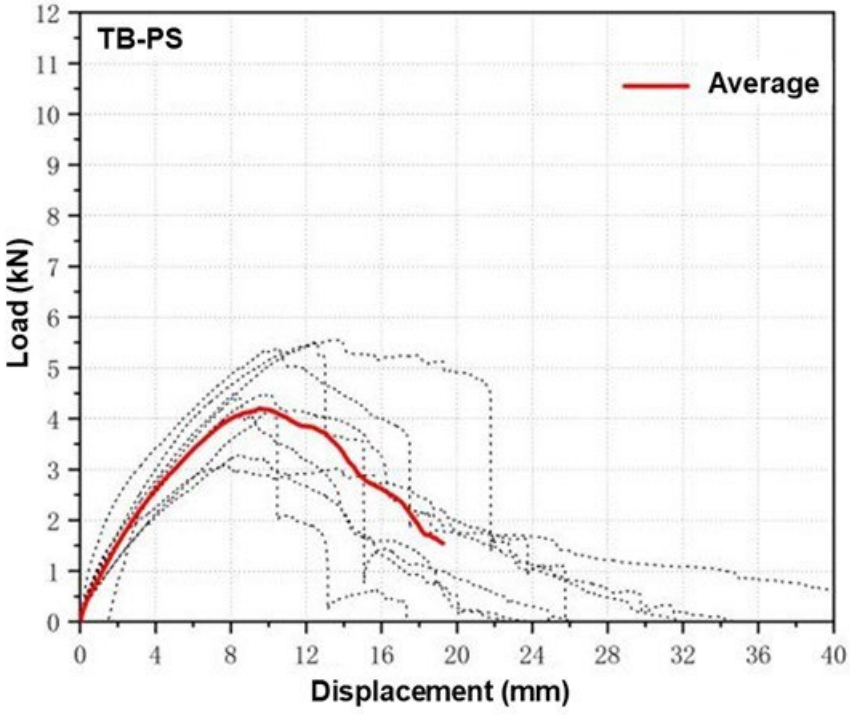
TB-PS
Average
Load (kN)
Displacement (mm)
0
1
2
3
4
5
6
7
8
9
10
11
12
0
4
8
12
16
20
24
28
32
36
40

(b)

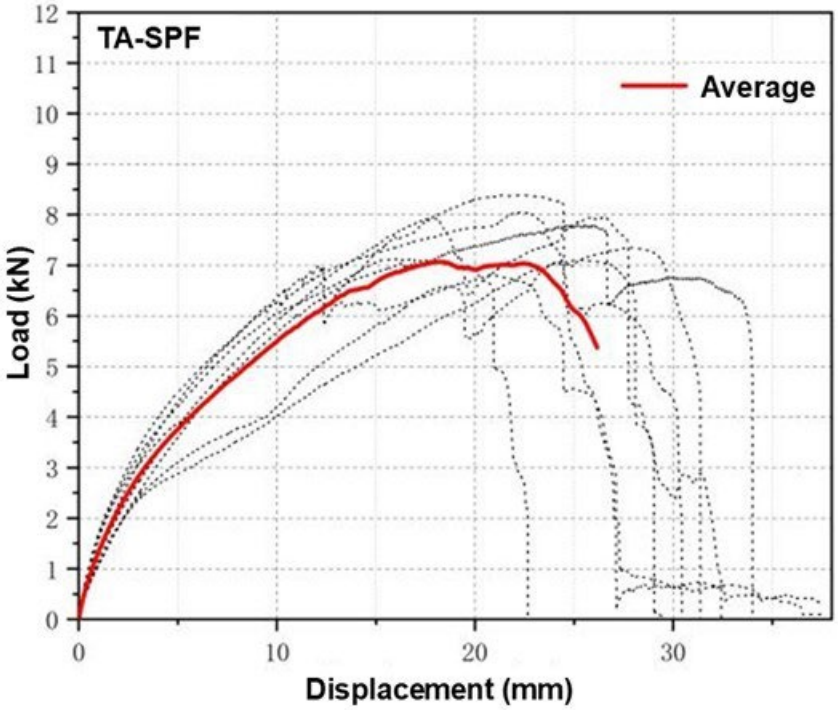
TA-SPF
Average
Load (kN)
Displacement (mm)
0
1
2
3
4
5
6
7
8
9
10
11
12
0
10
20
30

(c)

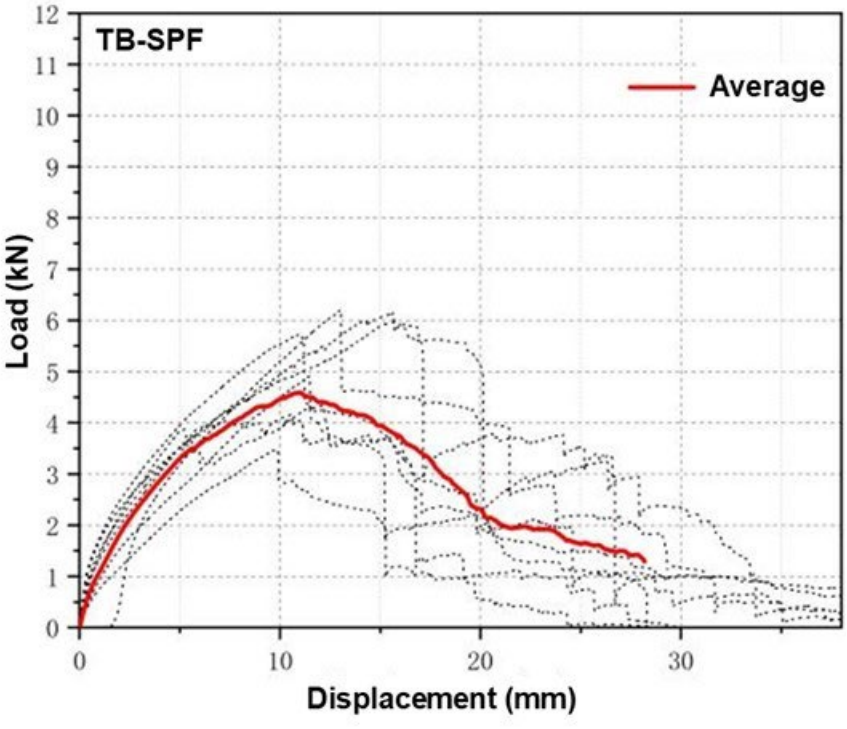
TB-SPF
Average
Load (kN)
Displacement (mm)
0
1
2
3
4
5
6
7
8
9
10
11
12
0
10
20
30

(d)

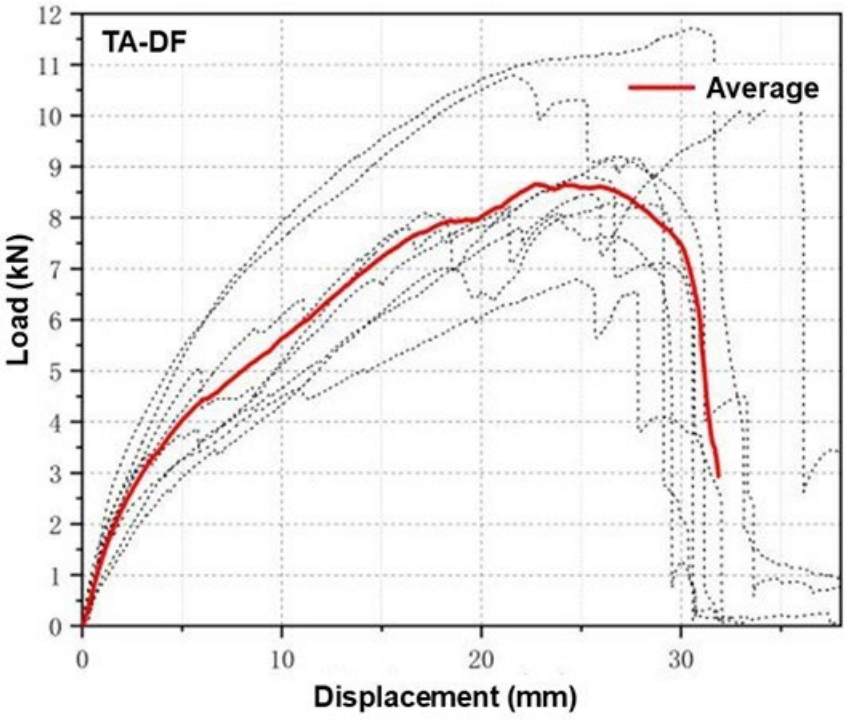

(e)

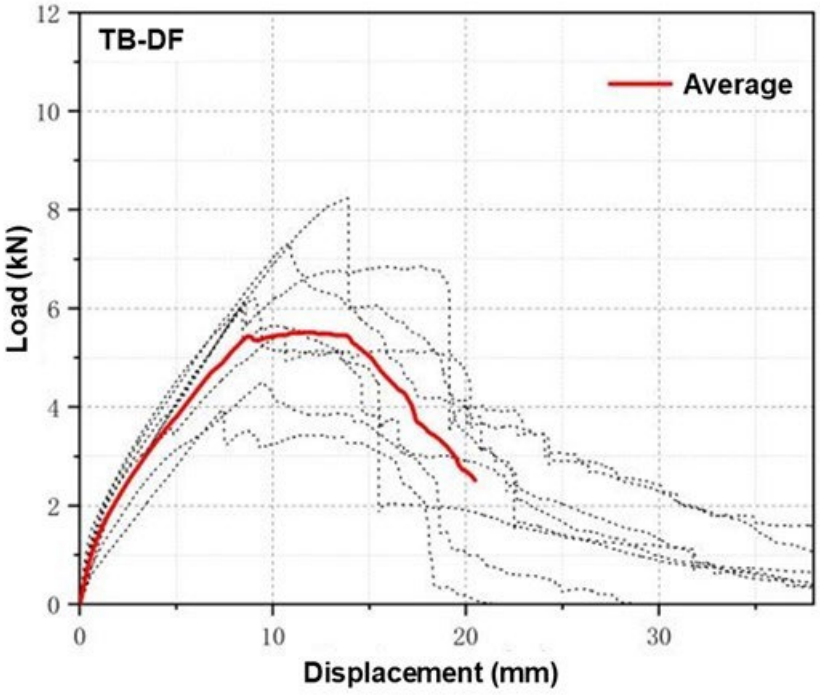

(f)

Fig. 4. Load-displacement curves for 6 types of configurations: (a) TA-PS: *Pinus sylvestris* L.+ Nails + A (metal- connector A); (b) TB-PS: *Pinus sylvestris* L.+ Nails + B; (c) TA-SPF: SPF + Nails + A; (d) TB-SPF: SPF + Nails + B; (e) TA-DF: Douglas fir + Nails + A; (f) TB-DF: Douglas fir + Nails + B

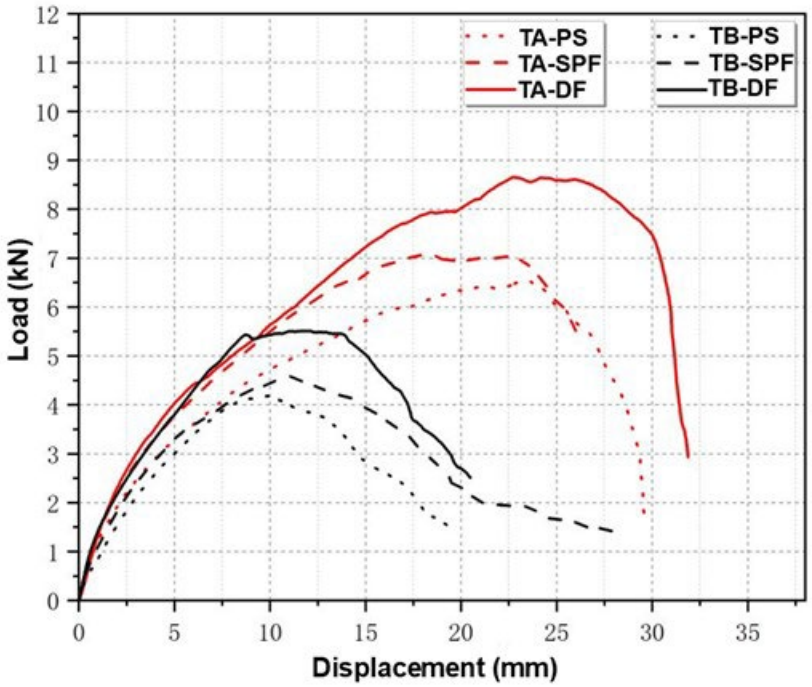

Fig. 5. Comparison of the average load-displacement curves for 6 types of configurations

Characteristic Values Analysis

Characteristic values analysis (CVA) is a reliably used method to analyze the load-displacement curve, and relevantly six typical eigenvalues of the specimen joints to be analyzed can be determined according to Fig. 6 (Hajmohammadi and Nourazar 2014; Seim *et al.* 2016; Hicks *et al.* 2019). Each eigenvalue is defined as follows:

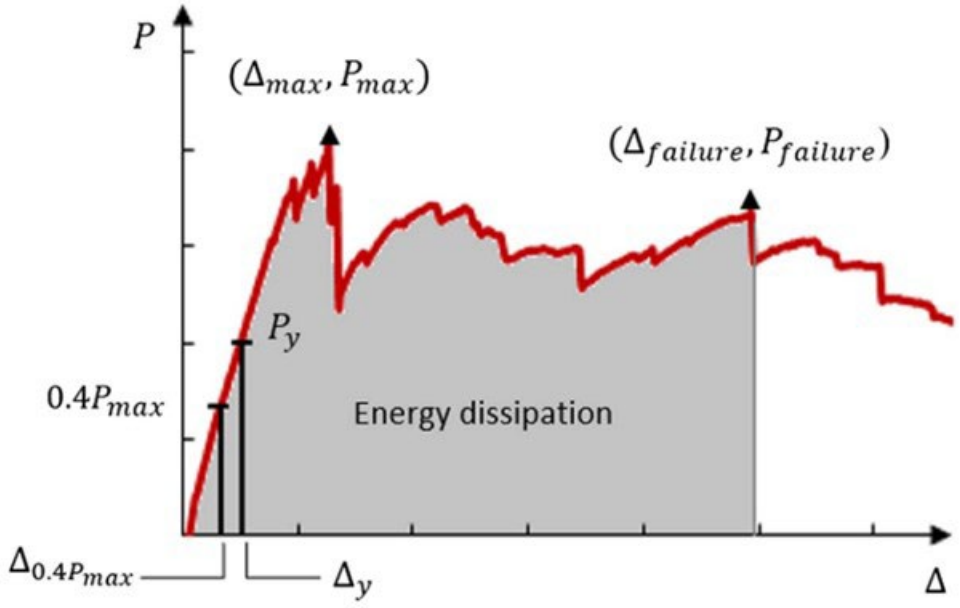

Fig. 6. Characteristic values analysis method

P_{max} stands for the maximum load at the highest point of load-displacement curve, which is an important indicator to measure the load capacity of specimens.

The yield load (P_y) and yield displacement ($\triangle_y$) represent the load and displacement of the specimen at yield, respectively. Both P_y and $\triangle_y$ can be determined by the general yield bending moment method (Fig. 7).

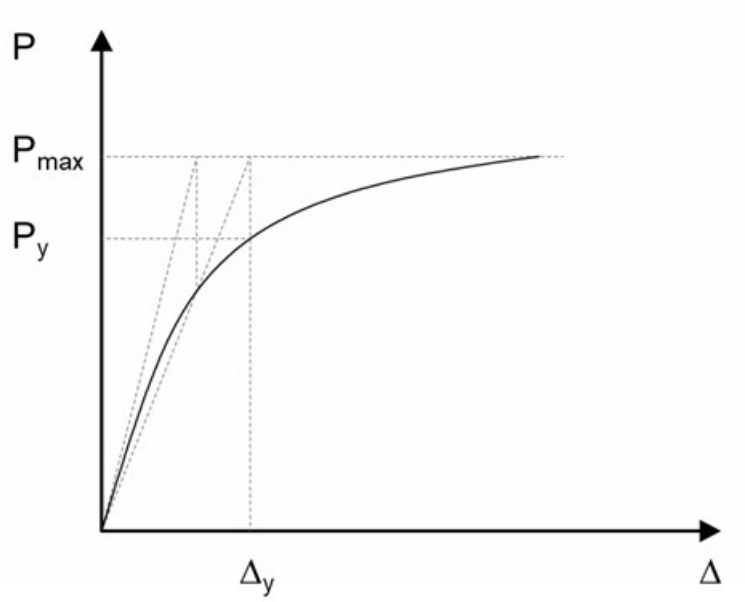

Fig. 7. General yield bending moment method

$P_{failure}$ represents the ultimate load, usually taking the value of the last maximum load before the joint completely destroyed or reaches 80% of the maximum load, and the corresponding $\Delta_{failure}$ represents the ultimate displacement. The two indicators are often used to represent the load capacity and deformation capacity of joints accordingly.

The value of J_{energy} is the area surrounded by the load-displacement curve in the coordinate axis, which is used to reflect the energy dissipation capacity of joints.

Ductility ratio (μ) is an indicator to evaluate the deformation capacity of joints, and the value is the ratio of the ultimate displacement $\triangle_{failure}$ to the yield displacement Δ_y. The calculation formula is shown in Eq. 1:

$$\mu = \Delta_{failure} / \Delta_y \quad (1)$$

In the CVA method, the ratio of 40% P_{max} in the load-displacement curve to the corresponding displacement ($\triangle_{0.4}$) is selected for the initial stiffness (K), and the calculation formula is shown in Eq. 2,

$$K = 0.4\,P_{max} / \Delta_{0.4} \quad (2)$$

where $0.4P_{max}$ is 40% of the maximum load (P_{max}) (kN), and $\triangle_{0.4}$ is the corresponding displacement (mm).

According to the CVA method, the bearing capacity, yield load, deformation capacity, energy dissipation capacity, ductility ratio, and initial stiffness of each group of

specimens were calculated. The average value and variation coefficient of the obtained eigenvalue are shown in Table 3.

According to Table 3, compared with other eigenvalues, the variation coefficient of ductility ratio and initial stiffness was numerically larger. The variation coefficient of each characteristic value of TA group was smaller than that of TB group. Combined with the failure mode of the two groups of specimens, the joint uplift performance of TB group was more variable and had a larger discrete trend under the combined effect of metal connectors and wood itself.

Table 3. Characteristic Values of the Six Specimen Configurations

Conf.	Average /Coefficient of Variation	Maximum Load	Yield Load	Deformation Capacity	Energy Dissipation	Ductility Ratio	Initial Stiffness
Index		P_{max} (kN)	P_y (kN)	$\triangle_{failure}$ (mm)	J_{energy} (kN·mm)	μ	K (kN·mm - 1)
TA-PS	Average	6.73	4.64	25.59	122.33	2.90	0.79
	Coefficient of variation	0.14	0.19	0.12	0.16	0.33	0.29
TA-SPF	Average	7.59	5.68	23.98	129.44	2.31	0.90
	Coefficient of variation	0.07	0.09	0.20	0.28	0.21	0.25
TA-DF	Average	9.27	6.26	29.15	187.10	3.36	0.91
	Coefficient of variation	0.17	0.30	0.10	0.24	0.60	0.30
TB-PS	Average	4.49	3.67	11.33	33.55	2.00	0.82
	Coefficient of variation	0.22	0.21	0.24	0.36	0.53	0.31
TB-SPF	Average	5.12	3.71	14.04	49.47	2.58	1.03
	Coefficient of variation	0.20	0.20	0.21	0.37	0.41	0.29
TB-DF	Average	6.06	4.75	14.37	60.03	2.25	1.05
	Coefficient of variation	0.24	0.26	0.23	0.34	0.35	0.26

Maximum load

To compare the eigenvalues between TA group and TB group in detail, TA-PS and TB-PS were used as a reference standard to compare the multiple relationship within TA and TB groups, as shown in Fig. 8. According to Fig. 8, the average value of the maximum load of the TA group was much larger than that of the TB group, which was nearly 1.5 times higher, indicating that the bearing capacity of the specimen using metal connector A was greater than that of the specimen using metal connector B under the same wood condition.

When utilizing the same metal-connector, the maximum load values from large to small were: Douglas fir, SPF, and *Pinus sylvestris* L.. In the TA group, the maximum load of TA-DF was 1.38 times that of TA-PS and 1.22 times that of TA-SPF; TA-SPF was 1.12 times that of TA-PS. In the TB group, the maximum load of TB-DF was 1.22 times that of TB-PS and 1.41 times that of TB-SPF; TB-SPF was 1.16 times that of TB-PS. Combined with the failure mode and load-displacement curves, it can be concluded that the bearing capacity and the capability of resisting screw-shear-force of Douglas fir were much larger than the other two kinds of wood. This is because the main failure mode of most specimens in the Douglas fir group was the brittle fracture of the screw, while the wood part contacted with the screw exhibited only slight tearing.

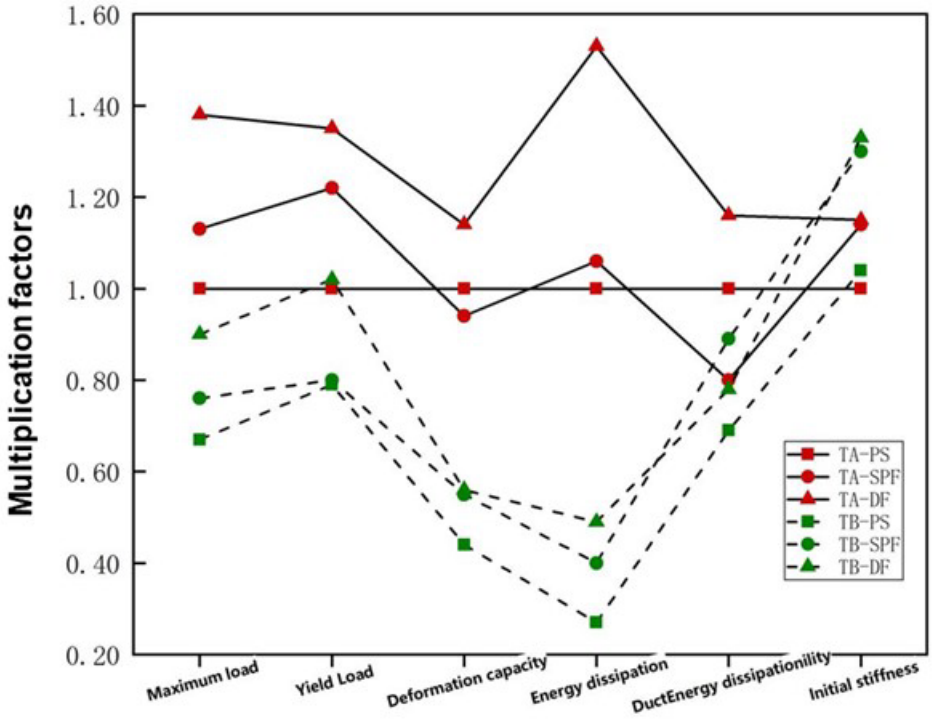

Fig. 8. The comparison of characteristic parameters taking group TA-PS as the reference value

According to Fig. 8, the maximum bearing capacity of *Pinus sylvestris* L. specimens in both TA group and TB group was smaller than that of the SPF specimens. Combined with the phenomenon of the failure modes, in terms of *Pinus sylvestris* L. specimens, the wood at the contact area between the specimen and the screw was torn in the form of blocks and gradually buckled, and then brittle failure occurred. As a result, the load increased rapidly, which means that the stiffness of the specimen was relatively small. For the SPF specimens, the wood at the contact area between the specimen and the screw was slowly pulled out in the form of fiber. Therefore, before the loading reached the maximum load, the load increase rate was relatively slow and the stiffness was larger. Therefore, the screw holding capability of *P. sylvestris* was greater but the stiffness was less than SPF, so the bearing capacity of *P. sylvestris* was less than SPF.

Yield load

The yield load is the critical value of the specimen to reach the yield point in the loading process, which is the maximum load that the specimen can withstand when the initial performance can be restored. The average yield load of the TA group was greater than that of TB group, indicating that the use of metal connector A had stronger resistance to load than metal connector B under the same wood condition.

In the TA group, the yield load of TA-DF was 1.35 times that of TA-PS and 1.1 times that of TA-SPF; TA-SPF was 1.22 times that of TA-PS. In the TB group, the yield load of TB-DF was 1.29 times that of TB-PS and 1.28 times that of TB-SPF. The yield load of TB-SPF and TB-PS were almost the same. The yield load of Douglas fir specimens was higher than other two groups, indicating that the Douglas fir specimens had better yield characteristics.

Deformation capacity

In terms of deformation capacity, the ultimate displacement is selected as the measurement standard. The ultimate displacement refers to the displacement value corresponding to the last maximum load before the specimen is completely destroyed. A larger ultimate displacement results in a stronger load resistance of the specimen. The average value of ultimate displacement of TA group was much larger than that of TB group, and the average increase under the same wood condition was 49%, indicating that the loading time of specimen using metal connector A was longer than that of specimen using metal connector B.

In the TA group, the deformation capacity of TA-DF was 1.22 times that of TA-PS and 1.14 times that of TA-SPF, and TA-SPF was slightly smaller than that of TA-PS. The deformation capacity of the TA-PS group was smallest, with the ultimate displacement value between 25 and 30 mm. In the TB group, the deformation capacity values of the three groups were not much different, between 10 to 15 mm, in which the displacement of TB-PS was the smallest, and the deformation capacity values of TB-DF and TB-SPF were 26.9% more than that of TB-PS.

Energy dissipation

Energy dissipation capacity is an important index to evaluate the performance of a joint. It refers to the area under the load-displacement curve surrounded by the X axis. A larger area results in greater energy dissipation capacity. The energy dissipation capacity of the TA group was much larger than that of TB group.

In the TA group, the energy dissipation capacity of TA-PS and TA-SPF specimens was similar, and the energy dissipation capacity of TA-DF was approximately 1.5 times that of the other two groups. The energy dissipation capacity of specimens in the TB group from large to small was TB-DF, TB-SPF, and TB-PS.

Ductility coefficient

Ductility coefficient refers to the ratio of ultimate displacement to yield displacement. A larger ductility coefficient results in a slower bearing capacity of the representative joint that decreases after reaching the yield point. In the TA group, the maximum ductility coefficient of TA-DF was 15.9% larger than that of TA-PS and 45.5% larger than that of TA-SPF. The results show that the ductility coefficient was proportional to the screw holding capability of wood.

In the TB group, the main failure modes of the joints were brittle failure and screw bending or brittle fracture was observed due to the crack propagation at the top beam plate. Although the nail holding force of SPF was smaller than that of the other two kinds of wood, the slow nail pulling occurred in the early stage of the loading process, which belonged to ductile failure. Therefore, the ductility coefficient of SPF group was larger.

The above analysis shows that different forms of metal connectors had different effects on the ductility of specimens. For Douglas-fir and *P. sylvestris* L. with strong screw holding capability, the ductility coefficient of specimens with A-type connector was higher, and the ductility coefficient of A-type connector was 49.3% and 45% higher than that of B-type connector. For SPF with poor screw holding capability, the ductility coefficient of specimens with B-type connector was higher.

Initial stiffness

The initial stiffness is the ratio between the yield load and the yield displacement of the specimens during the loading process. In the TA group, the initial stiffness of each

group was similar, and the initial stiffness of SPF and Douglas-fir specimens was slightly larger than that of *P. sylvestris* L. specimens. The initial stiffness values of SPF specimens and Douglas-fir specimens in TB group were similar, which were 14.5% higher than those of *P. sylvestris* L. specimens. This shows that the initial stiffness value of Douglas-fir and SPF specimens was larger using the same metal connector, and the initial stiffness value of TB specimens was greater than that of TA specimens under the same wood condition. It indicates that metal connector B was able to improve the initial stiffness value of joints more than metal connector A.

Foschi Formula Simulation Analysis

Foschi elastic-plastic theoretical model (Foschi *et al.* 1993; Bulleit 1995) is the theoretical expression of nonlinear load-displacement of metal connection joints proposed on the basis of nail connection tests, which is one of the most classical mechanical models in the study of metal connection joints in wood constructions. The basic principle of the Foschi model is to take two reference points in the same coordinate on the metal connector and the timber, and assume that the timber and the metal connector are rigid bodies, and they are connected by nonlinear springs. Each spring represents the interaction force between the timber and the metal connector, so as to express the nonlinear load-displacement relationship between the timber and the metal connector by the relative displacement of the two reference points under stress. The Foschi elasto-plastic load-displacement curve model is shown in Fig. 9, and the Foschi formula is shown in Eqs. 3 and 4.

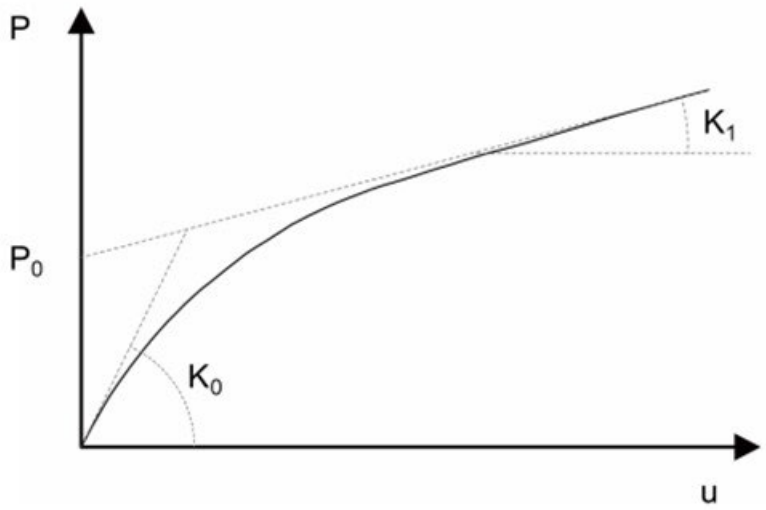

Fig. 9. Foschi load-displacement curve model

According to the literature research, there has been a lack of theoretical model simulation research on RTWC unidirectional load. Foschi model is a typical exponential function mathematical model, which can better express the force and displacement relationship of wood joints connected by nails and metal connectors. In this paper, the Foschi formula model was used to fit and analyze the force-displacement relationship of six groups of joints, which aimed to explore the accuracy of Foschi model to describe the

force-displacement relationship of such joints, and provide a theoretical basis for finite element numerical analysis.

$$P = (P_0 + K_1 u) \quad [1 - exp(-K_0 u / P_0)] \tag{3}$$

$$\lim_{\Delta \to 0} P'(u) = K_0 \tag{4}$$

where P is node load (N); P_0 is the load value (N) at the intersection of the yield stage asymptotic line and the coordinate axis; u is the node displacement (mm); K_0 is the initial stiffness (N / mm); and K_1 is the yield stiffness (N / mm).

The fitted curves for each group are shown in Fig. 10, and the fitted parameters are shown in Table 4. The fitting results of six groups show that the fitting curves were similar to the trend of the test curves for the most part, and the fitted R-Square was greater than 0.900 in all groups, which indicates that the Foschi formula was suitable for the simulation of unidirectional load of such nodes. Due to the large dispersion of wood materials and the aberration of data obtained from the test, the value of fitting parameter K_0 in each group indicates that the initial stiffness of each joint was not highly correlated with the form of wood or metal connectors. The post-yield stiffness K_0 was larger in the TB group than in the TA group.

Table 4. The Fitted Parameters of Foschi Formula in Each Group

Index		P_0/N	K_0 / (N·mm - 1)	K_1 / (N·mm - 1)	R-Squared
TA	PS	3765	1197	110	0.93
	SPF	3664	1457	169	0.95
	DF	4853	1219	153	0.98
TB	PS	2569	1133	150	0.96
	SPF	2494	1495	161	0.92
	DF	3220	1604	199	0.96

An improved mathematical model based on the Foschi formula, which was able to apply the case before joints reaching the limit displacement, was offered by Folz and Foschi (1989, 1990, 1991). When the displacement value was greater than the limit displacement and less than the failure displacement, Folz gave the linear fitting function of the failure stage. When the displacement exceeded the failure displacement, the load value was 0. Folz's mathematical model is shown in Eq. 5,

$$P = \begin{cases} (P_0 + K_1 * u) \times [1 - \exp(-K_0 \times u / P_0)] \; u < u_{\mathrm{m}} \\ P_{\mathrm{m}} + K_2 (u - u_{\mathrm{m}}) \; u_{\mathrm{m}} \le u < u_{\mathrm{d}} \\ 0 \; u > u_{\mathrm{d}} \end{cases} \tag{5}$$

where P is node load (N); P_{m} is ultimate load (N); u is the node displacement (mm); u_{m} is the ultimate displacement (mm); u_{d} is failure displacement (mm); K_0 is initial stiffness (N / mm); K_1 is yield stiffness (N / mm); K_2 is degradation stiffness (N / mm); and P_0 is the load value (N) at the intersection of the yield stage asymptotic line and the coordinate axis.

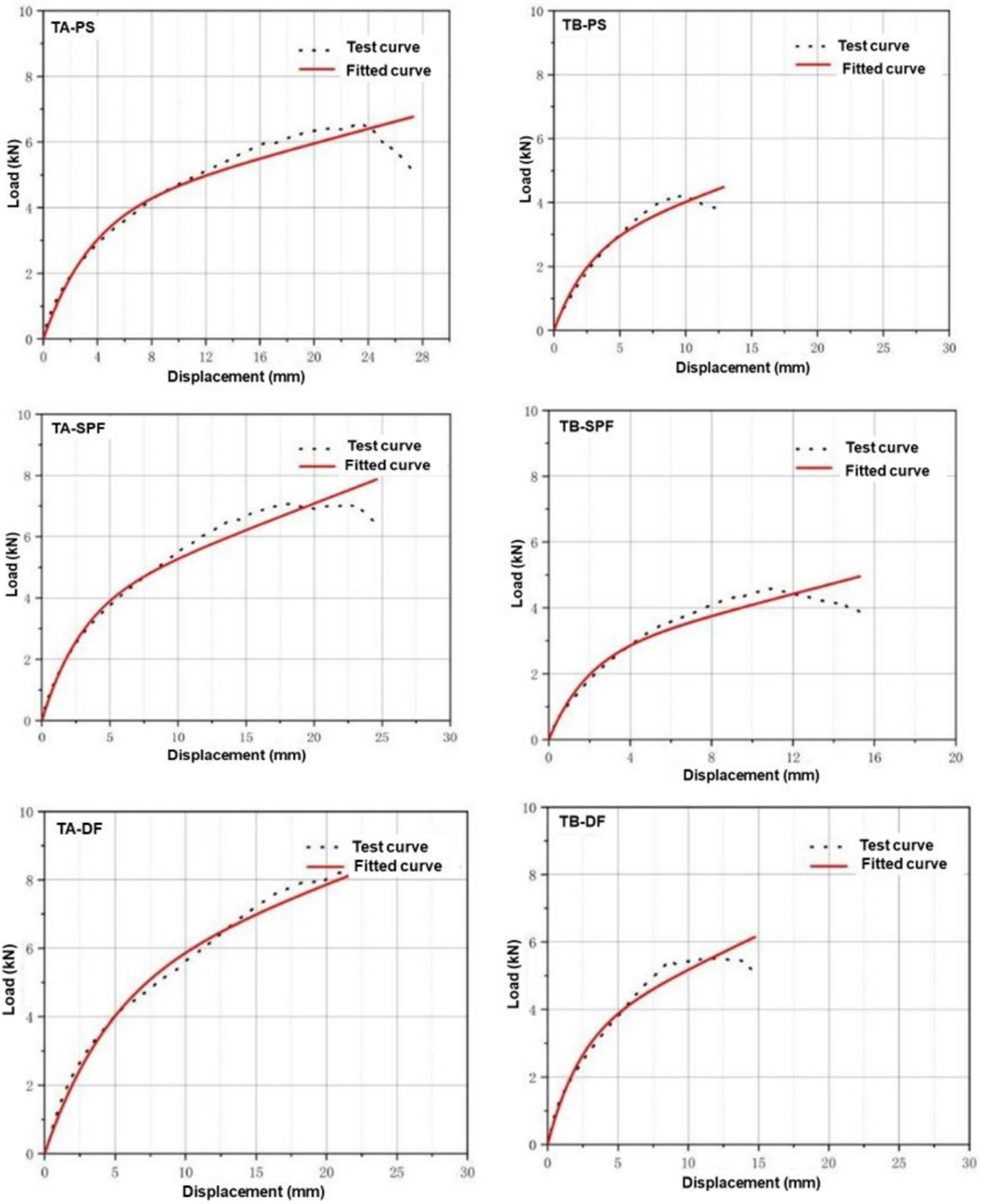

Fig. 10. Comparison of test curves and fitting curves

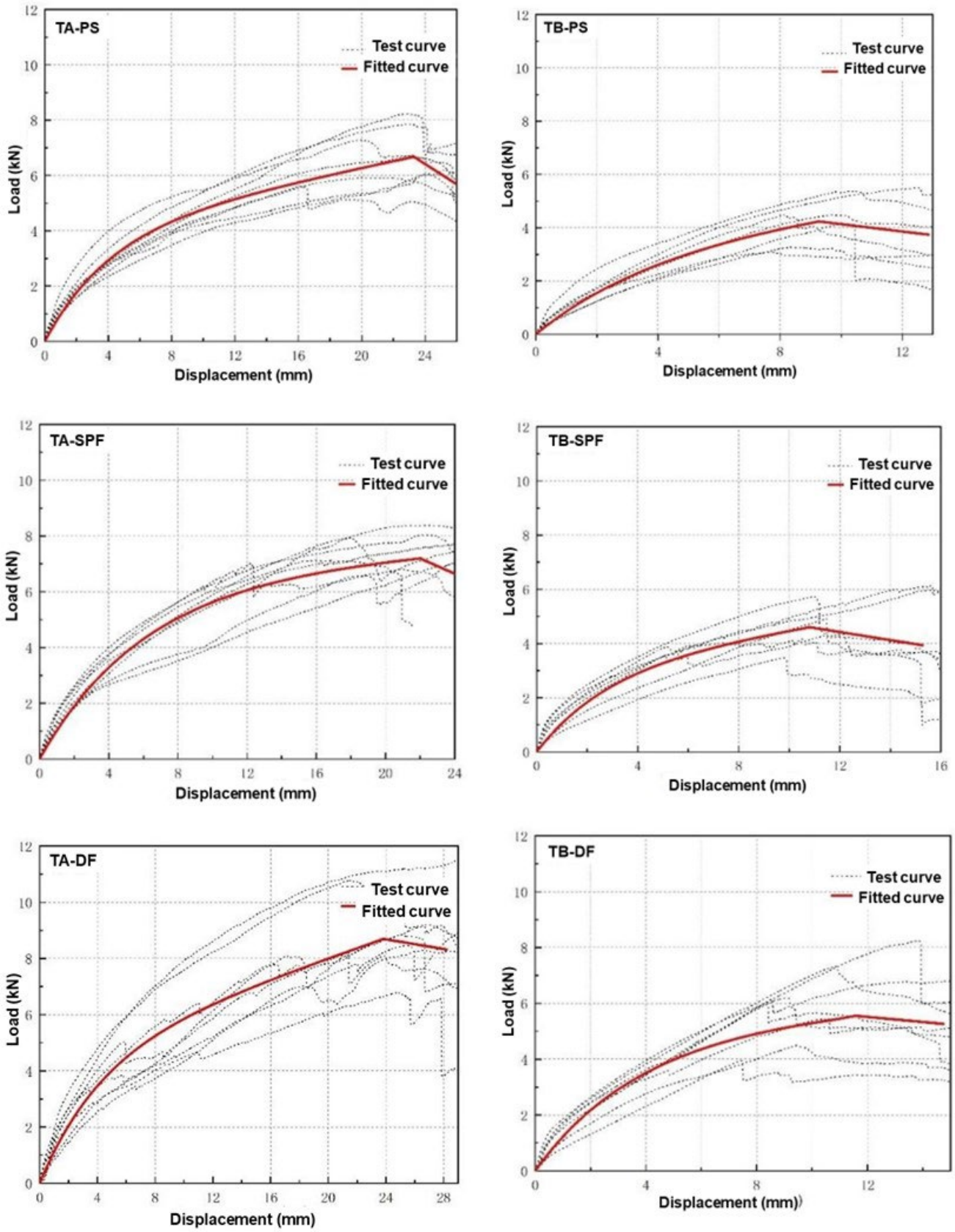

Fig. 11. Comparison of Foschi fitting curves and test curves of each joint

McCarthy and Little (1988) proposed a method to determine the parameters in the Folz model, considering two ranges to define K_0, K_1, and P_0 In the yield displacement range, $K_1 = 0$, P_0 was the yield point load; $K_1 \neq 0$, P_0 was the tangent intercept at the yield point. At the maximum load or near the maximum limit displacement, $K_1 = 0$, P_0 was the maximum load; $K_1 \neq 0$, P_0 was the maximum load tangent intercept.

According to Eq. 5 and the parameter determination method of McCarthy and Little (1988), the parameters obtained by data fitting of the load-displacement curves of six groups of joints are shown in Table 5 and the data fitting curves are shown in Fig. 11.

Table 5. Foschi Parameter Values of Each Metal Connection Joints

Index		P_m (N)	u_m (mm)	u_d (mm)	P_0 (N)	K_0/ (N·mm^{-1})	K_1 (N·mm^{-1})	K_2 (N·mm^{-1})
TA	PS	6675	23	27	3905	1077	119	-367
	SPF	7199	22	24	6441	1104	42	-274
	DF	8691	24	28	4459	1231	178	-101
TB	PS	4243	9	13	3122	943	150	-138
	SPF	4609	11	15	3027	1211	151	-150
	DF	5539	11	15	4993	1374	66	-91

Through comparing the test curves and fitting curves of each group, the fitting curves of each group were found to be between the maximum values of the test curve, which can better express the load-displacement variation characteristics of RTWC joints under unidirectional load. The fitting curves had good applicability in the elastic stage and elastic-plastic stage of each group, and the fitting curves in the failure stage were consistent with the trend of the test curve. It shows that the improved expression based on the Foschi formula was suitable for the simulation of the unidirectional load-displacement curve of RTWC joints of the wooden structure connected by the metal connector. The empirical formulas of six RTWC joints in the experiment can be obtained by substituting the parameters obtained in Table 5 into Eq. 5, as shown in Eqs. 6 through 11.

TA-PS:

$$P = \begin{cases} (3905 + 119 \times u) \times [1 - \exp(-1077 \times u/3905)] & u < 23 \\ 6675 - 367(u - 23) & 23 \leq u < 27 \\ 0 & u > 27 \end{cases} \quad (6)$$

TA-SPF:

$$P = \begin{cases} (6441 + 42 \times u) \times [1 - \exp(-1104 \times u/6441)] & u < 22 \\ 7199 - 274(u - 22) & 22 \leq u < 26 \\ 0 & u > 26 \end{cases} \quad (7)$$

TA-DF:

$$P = \begin{cases} (4459 + 178 \times u) \times [1 - \exp(-1231 \times u/4459)] & u < 24 \\ 8691 - 101(u - 24) & 24 \leq u < 28 \\ 0 & u > 28 \end{cases} \quad (8)$$

TB-PS:

$$P = \begin{cases} (3122 + 150 \times u) \times [1 - \exp(-943 \times u/3122)] & u < 9 \\ 4243 - 138(u - 9) & 9 \le u < 13 \\ 0 & u > 13 \end{cases} \quad (9)$$

TB-SPF:

$$P = \begin{cases} (3027 + 151 \times u) \times [1 - \exp(-1211 \times u/3027)] & u < 11 \\ 4609 - 150(u - 11) & 11 \le u < 15 \\ 0 & u > 15 \end{cases} \quad (10)$$

TB-DF:

$$P = \begin{cases} (4993 + 66 \times u) \times [1 - \exp(-1374 \times u/4993)] & u < 11 \\ 5539 - 91(u - 11) & 11 \le u < 15 \\ 0 & u > 15 \end{cases} \quad (11)$$

CONCLUSIONS

1. During the test of RTWC joints connected with metal parts, the specimen with metal connector B reached the ultimate bearing capacity earlier than that with metal connector A. The maximum load, yield load, ultimate displacement, and energy dissipation capacity of specimens with metal connector B were lower than those of specimens with metal connector A, and the variability was large, indicating that the connection performance of specimens with metal connector A was better than that of specimens with metal connector B in the experiment.
2. In the test of specimens connected by metal connector A, the damage mode of the DF group specimens was mainly due to the brittle fracture of the screws, and the damage mode of the PS and SPF group specimens was mainly due to nail pulling, bending of the nail rod, and shearing of the wood at the top joint; the damage of the three specimens connected by metal connector B was basically the same, mainly due to the bending of the top nail rod and severe splitting of the wood at the top plate.
3. Under the same metal connection, the maximum load and energy dissipation capacity of specimens using the same metal connector showed the following rules: DF group > SPF group > PS group. With the exception of the ductility coefficient of TB-DF group being low, the characteristic values of DF group specimens were the highest, indicating that the performance of DF type specimens was the best. When using metal connector A, the maximum load, yield load, energy dissipation capacity, and initial stiffness of SPF group were higher than those of PS group; when metal connector B was used, the maximum load, ultimate displacement, energy dissipation capacity, ductility coefficient, and initial stiffness of SPF group were greater than those of PS group.
4. Among the three wood specimens, the metal connector had the highest degree of improvement in the mechanical characteristics of SPF RTWC joints.
5. The Foschi parameter values of six kinds of RTWC metal joints under unidirectional load were determined by experiments, and the applicability of Foschi and Folz

improved load-displacement theoretical models was verified. Finally, the relevant empirical formulas of six groups of RTWC joints in the test were established according to the model.

ACKNOWLEDGMENTS

Special thanks to following for their research support: National Natural Science Foundation of China (31860184); Young Talents of Science and Technology in Universities of Inner Mongolia Autonomous Region (NJYT-20-A15); Inner Mongolia Science and Technology Major Projects (CGZH2018135); and Inner Mongolia Grassland Talent Team, Innovation Talent Team (TC2019071720712).

REFERENCES CITED

Alhawamdeh, B., and Shao, X. (2021). "Fatigue performance of wood frame roof-to-wall connections with elastomeric adhesives under uplift cyclic loading," *Engineering Structures* 229, article ID 111602. DOI: 10.1016/j.engstruct.2020.111602

Alhawamdeh, B., and Shao, X. (2020). "Uplift capacity of light-frame rafter to top plates connections applied with elastomeric construction adhesives," *Journal of Materials in Civil Engineering* 32(5), article ID 04020078. DOI: 10.1061/(ASCE)MT.1943-5533.0003152

Arriaga, F., Iniguez-Gonzalez, G., Esteban, M., and Divos, F. (2012). "Vibration method for grading of large cross-section coniferous timber species," *Holzforschung* 66(3), 381-387. DOI: 10.1515/HF.2011.167

ASTM D1761 (2006). "Standard test methods for mechanical fasteners in wood," ASTM International, West Conshohocken, PA, USA.

ASTM D1761-12 (2012). "Standard test methods for mechanical fasteners in wood," ASTM International, West Conshohocken, PA, USA.

Building Performance Assessment Report (1999). *Hurricane Georges in Puerto Rico: Observations, Recommendations, and Technical Guidance* (FEMA 339), U. S. Federal Emergency Management Agency, Mitigation Directorate, Washington, DC, USA.

Bekhta, P., Proszyk, S., Lis, B., and Krystofiak, T. (2014). "Gloss of thermally densified alder (*Alnus glutinosa* Goertn.), beech (*Fagus sylvatica* L.), birch (*Betula verrucosa* Ehrh.), and pine (*Pinus sylvestris* L.) wood veneers," *European Journal of Wood and Wood Products* 72(6), 799-808. DOI: 10.1007/s00107-014-0843-3

Bulleit, W. M. (1995). "Applications in timber structures," in: *Probabilistic Structural Mechanics Handbook*, C. Sundararajan (ed.), Springer, Boston, MA, USA, pp. 684-706. DOI: 10.1007/978-1-4615-1771-9_29

Burawska-Kupniewska, I., Krzosek, S., Mankowski, P., Grzeskiewicz, M., and Mazurek, A. (2019). "The influence of pine logs (*Pinus sylvestris* L.) quality class on the mechanical properties of imtber," *BioResources* 14(4), 9287-9297. DOI: 10.15376/biores.14.4.9287-9297

Buyuksari, U., As, N., and Dundar, T. (2017). "Mechanical properties of earlywood and latewood sections of scots pine wood," *BioResources* 12(2), 4004-4012. DOI: 10.15376/biores.12.2.4004-4012

Cai, S., Jebrane, M., Terziev, N., and Daniel, G. (2016). "Mechanical properties and decay resistance of Scots pine (*Pinus sylvestris* L.) sapwood modified by vinyl acetate-epoxidized linseed oil copolymer," *Holzforschung* 70(9), 885-894. DOI: 10.1515/hf-2015-0248

Cheng, J. (2004). "Testing and analysis of the toe-nailed connection in the residential roof-to-wall system," *Forest Products Journal* 54(4), 58-65.

Di, J., and Zuo, H. (2021). "Experimental and reliability-based investigation on sheathing-to-framing joints under monotonic and cyclic loads," *Forests* 12(8), article no. 995. DOI: 10.3390/f12080995

Dong, W., Wang, Z., Zhou, J., and Gong, M. (2021). "Experimental study on bending properties of cross-laminated timber-bamboo composites," *Construction and Building Materials* 300, article ID 124313. DOI: 10.1016/j.conbuildmat.2021.124313

Edmonson, W. C., Schiff, S. D., and Nielson, B. G. (2012). "Behavior of light-framed wood roof-to-wall connectors using aged lumber and multiple connection mechanisms," *Journal of Performance of Constructed Facilities* 26(1), 26-37. DOI: 10.1061/(ASCE)CF.1943-5509.0000201

Ekman, B. R., Willför, S., Sjöholm, R., Reunanen, M., Måki, J., Lehtilå, R., and Eckerman, C. (2002). "Identification of the lignan nortrachelogenin in knot and branch heartwood of Scots pine (*Pinus sylvestris* L.)," *Holzforschung* 56(3), 253-256. DOI: 10.1515/HF.2002.041

Folz, B., and Foschi, R. O. (1989). "Reliability-based design of wood structural systems," *ASCE Journal of the Structural Division* 115(7), 1666-1680.

Folz, B., and Foschi, R. O. (1990). "Reliability of timber beams subjected to ponding," *ASCE Journal of the Structural Division* 116(2): 490-499.

Folz, B., and Foschi, R.O. (1991). "Coupled vibration response of floor system with occupants," *ASCE Journal of the Engineering Mechanics Division* 117(4), 872-892.

Foschi, R. O., Folz, B., and Yao, F. (1993). "Reliability-based design of wood structures: Background to CSA-086.1-M89," *Canadian Journal of Civil Engineering* 20, 349-357.

Gong, M., Delahunty, S., and Chui, Y. H. (2014). "Influence of number of finger joints per stud on mechanical performance of wood shearwalls," *Construction and Building Materials* 50, 335-339. DOI: 10.1016/j.conbuildmat.2013.09.041

Guha, T. K., and Kopp, G. A. (2014). "Storm duration effects on roof-to-wall-connection failures of a residential, wood-frame, gable roof," *Journal of Wind Engineering and Industrial Aerodynamics* 133(SI), 101-109. DOI: 10.1016/j.jweia.2014.08.005

Hajmohammadi, M. R. and Nourazar, S. S. (2014). "On the solution of characteristic value problems arising in linear stability analysis; semi analytical approach," *Applied Mathematics and Computation* 239, 126-132. DOI: 10.1016/j.amc.2014.04.060

Henderson, D. J, Morrison, M. J., and Kopp, G. A. (2013). "Response of toe-nailed, roof-to-wall connections to extreme wind loads in a full-scale, timber-framed, hip roof," *Engineering Structures* 56, 1474-1483. DOI: 10.1016/j.engstruct.2013.07.001

Hicks, M., Varkey, D., Van den Eijnden, A., De Gast, T., and Vardon, P. J. (2019). "On characteristic values and the reliability-based assessment of dykes," *Georisk: Assessment and Management of Risk for Engineered Systems and Geohazards* 13(4), 313-319. DOI: 10.1080/17499518.2019.1652918

Korkut, S., Akguel, M., and Duendar, T. (2008). "The effects of heat treatment on some technological properties of Scots pine (*Pinus sylvestris* L.) wood," *Bioresource Technology* 99(6), 1861-1868. DOI: 10.1016/j.biortech.2007.03.038

McCarthy, M., and Little, J. K. (1988). "Sensitivity of truss plate model parameters to parameter determination methods," *Forest Products Journal* 38(5), 63-67.

Megnis, M., Olsson, T., Varna, J., and Lindberg, H. (2002). "Mechanical performance of linseed oil impregnated pine as correlated to the take-up level," *Wood Science and Technology* 36(1), 1-18. DOI: 10.1007/s002260100120

Morrison, M. J., Kopp, G. A., Gavanski, E., Miller, C., and Ashton, A. (2014). "Assessment of damage to residential construction from the tornadoes in Vaughan, Ontario, on 20 August 2009," *Canadian Journal of Civil Engineering* 41(6), 550-558. DOI: 10.1139/cjce-2013-0570

Rautiainen, R., and Alen, R. (2007). "Papermaking properties of the ECF-bleached kraft pulps from first-thinning Scots pine (*Pinus sylvestris* L.)," *Holzforschung* 61(1), 8-13. DOI: 10.1515/HF.2007.002

Sarkhad, M., Ishiguri, F., Nezu, I., Tumenjargal, B., Takahashi, Y., Baasan, B., Chultem, G., Ohshima, J., and Yokota, S. (2020). "Preliminary evaluation for quality of dimension lumber in four common softwoods in Mongolia," *Journal of Wood Science* 66(1), article no. 72. DOI: 10.1186/s10086-020-01919-7

Satheeskumar, N., Henderson, D. J., Ginger, J. D., and Wang, C. (2017). "Three-dimensional finite-element modeling and validation of a timber-framed house to wind loading," *Journal of Structural Engineering* 143(9), article ID 04017112. DOI: 10.1061/(ASCE)ST.1943-541X.0001850

Seim, W., Kramar, M., Pazlar, T., and Vogt, T. (2016). "OSB and GFB as sheathing materials for timber-framed shear walls: Comparative study of seismic resistance," *Journal of Structural Engineering* 142(4), article ID E4015004. DOI: 10.1061/(ASCE)ST.1943-541X.0001293

Shanmugam, B., Nielson, B. G., and Prevatt, D. O. (2009). "Statistical and analytical models for roof components in existing light-framed wood structures," *Engineering Structures* 31(11), 2607-2616. DOI: 10.1016/j.engstruct.2009.06.009

Shanmugam, B., Nielson, B. G., and Schiff, S. D. (2011). "Multi-axis treatment of typical light-frame wood roof-to-wall metal connectors in design," *Engineering Structures* 33(12), 3125-3135. DOI: 10.1016/j.engstruct.2011.07.031

Shen, Y., Zhang, X., He, Q., Wang, X., Wang, Z., Yang, J., Chen, Z., Yu, J., Duo, H., and Wang, X. (2020). "Study of VOCs release during drying of plantation-grown *Pinus sylvestris* and naturally grown Russian *Pinus sylvestris*," *Journal of Wood Science* 66(1), article no. 34. DOI: 10.1186/s10086-020-01882-3

Sobierajska, K., Wachowiak, W., Zaborowska, J., Łabiszak, B., Wójkiewicz, B., Sekiewicz, M., Jasinska, A. K., Sekiewicz, K., Boratynska, K., Marcysiak, K., *et al.* (2020). "Genetic consequences of hybridization in relict isolated trees *Pinus sylvestris* and the *Pinus mugo* complex," *Forests* 11(10), Article Number 1068. DOI: 10.3390/f11101086

Simsek, H., Baysal, E., and Peker, H. (2010). "Some mechanical properties and decay resistance of wood impregnated with environmentally-friendly borates," *Construction and Building Materials* 24(11), 2279-2284. DOI: 10.1016/j.conbuildmat.2010.04.028

Stevenson, S. A., Ansary, A. M. E., and Kopp, G. A. (2019). "A practical modelling technique to assess the performance of wood-frame roofs under extreme wind loads," *Engineering Structures* 191, 640-648. DOI: 10.1016/j.engstruct.2019.04.058

Stoner, M., and Pang, W. (2021). "Tornado hazard assessment of residential structures built using cross-laminated timber and light-frame wood construction in the US," *Natural Hazards Review* 22(4), article ID 04021032. DOI: 10.1061/(ASCE)NH.1527-6996.0000490

Temiz, A., Gezer, E. D., Yildiz, U. C., and Yildiz, S. (2008). "Combustion properties of alder (*Alnus glutinosa* L.) *Gaertn.* subsp. *barbata* (C.A. Mey) Yalt.) and southern pine (*Pinus sylvestris* L.) wood treated with boron compounds," *Construction and Building Materials* 22(11), 2165-2169. DOI: 10.1016/j.conbuildmat.2007.08.011

Van de Lindt, J. W., Graettinger, A., Gupta, R., Skaggs, T., Pryor, S., and Fridley, K. J. (2007). "Performance of wood-frame structures during Hurricane Katrina," *Journal of Performance of Constructed Facilities* 21(2), 108-116. DOI: 10.1061/(ASCE)0887-3828(2007)21:2(108)

Wang, J., Pang, W., Cao, S., Zhou, Q., and Liao, H. (2019a). "Fragility analysis of the roof structure of low-rise buildings subjected to tornado vortices," *Construction and Building Materials* 189, 45-55. DOI: 10.1016/j.jweia.2019.03.006

Wang, X., Zhou, A., Zhao, L., and Chui, Y. H. (2019b). "Mechanical properties of wood columns with rectangular hollow cross section," *Construction and Building Materials* 214, 133-142. DOI: 10.1016/j.conbuildmat.2019.04.119

Wang, Z., Fu, H., Gong, M., Luo, J., Dong, W., Wang, T., and Chui, Y. H. (2017). "Planar shear and bending properties of hybrid CLT fabricated with lumber and LVL," *Construction and Building Materials* 151, 172-177. DOI: 10.1016/j.conbuildmat.2017.04.205

Witomski, P., Krajewski, A., and Kozakiewicz, P. (2014). "Selected mechanical properties of Scots pine wood from antique churches of Central Poland," *European Journal of Wood and Wood Products* 72(2), 293-296. DOI: 10.1007/s00107-014-0783-y

Xiao, Y., Cai, H., and Dong, S. Y. (2021). "A pilot study on cross-laminated bamboo and timber beams," *Journal of Structural Engineering* 147(4), article ID 06021002. DOI: 10.1061/(ASCE)ST.1943-541X.0002916

Xiao, Q., Doudak, G., and Mohareb, M. (2017). "Numerical and experimental investigation of lateral torsional buckling of wood beams," *Construction and Building Materials* 151, 85-92. DOI: 10.1016/j.engstruct.2017.08.020

Yildiz, U. C., Temiz, A., Gezer, E. D., and Yildiz, S. (2004). "Effects of the wood preservatives on mechanical properties of yellow pine (*Pinus sylvestris* L.) wood," *Building and Environment* 39(9), 1071-1075. DOI: 10.1016/j.buildenv.2004.01.032

Yin, Y., and Li, Y. (2011). "Probabilistic loss assessment of light-frame wood construction subjected to combined seismic and snow loads," *Engineering Structures* 33(2), 380-390. DOI: 10.1016/j.engstruct.2010.10.018

Zhang, Y., and Cai, L. (2008). "Impact of heating speed on permeability of sub-alpine fir," *Wood Science and Technology* 42(3), 241-250. DOI: 10.1007/s00226-007-0172-3

Zhang, R., Zhang, J., Guo, W., Wu, Z., Wang, Z., and Yang, B. (2021). "Effect of torrefaction pretreatment on biomass chemical looping gasification (BCLG) characteristics: Gaseous products distribution and kinetic analysis," *Energy Conversion and Management* 237, article ID 114100. DOI: 10.1016/j.enconman.2021.114100

Zheng, W., Lu, W., Liu, W., Wang, L., and Ling, Z. (2015). "Experimental investigation of laterally loaded double-shear-nail connections used in midply wood shear walls," *Construction and Building Materials* 101(1), 761-771. DOI: 10.1016/j.conbuildmat.2015.10.100

Zhou, S. C., Demartino, C., and Xiao, Y. (2020). "High-strain rate compressive behavior of Douglas fir and glubam," *Construction and Building Materials* 258, article ID 119466. DOI: 10.1016/j.conbuildmat.2020.119466

Article submitted: March 28, 2022; Peer review completed: June 4, 2022; Revised version received and accepted: June 5, 2022; Published: June 10, 2022.
DOI: 10.15376/biores.17.3.4532-4558